Journal of Alloys and Compounds 506 (2010) 631–639

Contents lists available at ScienceDirect

Journal of Alloys and Compounds

journal homepage: www.elsevier.com/locate/jallcom

Structural, mechanical and tribological properties of A356 aluminium alloy reinforced with Al_2O_3, SiC and SiC + graphite particles

Aleksandar Vencl[a,*], Ilija Bobic[b], Saioa Arostegui[c], Biljana Bobic[d], Aleksandar Marinković[a], Miroslav Babić[e]

[a] Tribology Laboratory, Mechanical Engineering Faculty, University of Belgrade, Kraljice Marije 16, 11120 Belgrade 35, Serbia
[b] Institute of Nuclear Science "Vinca", Mike Petrovića Alasa 12-14, 11001 Belgrade, Serbia
[c] CSM Instruments SA, Rue de la Gare 4, CH-2034 Peseux, Switzerland
[d] R&D Center IHIS Techno-Experts, Batajnički put 23, 11080 Belgrade, Serbia
[e] Tribology Center, Mechanical Engineering Faculty, University of Kragujevac, Sestre Janjić 6, 34000 Kragujevac, Serbia

ARTICLE INFO

Article history:
Received 7 June 2010
Accepted 2 July 2010
Available online 14 July 2010

Keywords:
A356 alloy
Metal matrix composites
Compocasting
Microstructure
Wear
Friction

ABSTRACT

Particulate composites with A356 aluminium alloy as a matrix were produced by compocasting process using ceramic particles (Al_2O_3, SiC) and graphite particles. The matrix alloy and the composites were thermally processed applying the T6 heat treatment regime. Structural, mechanical and tribological properties of heat treated matrix alloy and the composites were examined and compared. It was shown that heat treatment affected microstructure of the composites matrix. The fracture of the composites matrix was ductile, while transition from ductile to brittle fracture occurred in the zone of reinforcing particles. The values of elasticity modulus of all the composites were higher in relation to the matrix alloy. It was also established that wear resistance and coefficient of friction were better at the SiC particulate composites than at the Al_2O_3 particulate composite, while the addition of graphite particles improved tribological properties further.

1. Introduction

A356 aluminium alloy is a casting alloy consisting of aluminium, silicon and magnesium. It is distinguished by good mechanical characteristics and high ductility, as well as excellent casting characteristics and high corrosion resistance. Mechanical properties of this alloy can be significantly improved by suitable heat treatment and especially using T6 heat treatment regime [1]. The alloy has been widely applied in the machinery, aircraft and defence industries and particularly in the automotive industry to replace steel components [2]. A356 aluminium alloy has been also used as the basis for obtaining composites with ceramic reinforcing particles and fibres such as SiC, Al_2O_3 etc. [3–5] aiming to improve the alloy wear resistance.

Starting from the first experiments [6] until today [7] the process of obtaining composites named compocasting is an object of interest for many researchers from the whole world. Belonging to the SST (semi-solid technology) procedures for composites production this process is based on the infiltration (with mixing) of reinforcing particles and/or fibres in the semi-solid melt of an alloy. Compocasting shows some advantages in relation to other processes for producing composites, when the composite matrix is in liquid state. This process is performed at considerably lower temperatures and an extended life of tools can be achieved [8] as well as energy savings. Accordingly, the process is of lower cost [9] compared to other procedures of composites production.

Particulate reinforced composites cost less than fibre reinforced composites, owing to the lower costs of the particles. In addition, mechanical and physical properties of particulate composites are generally isotropic. Cast metal matrix particulate composites represent the lowest cost composites, and they find the most tribological applications [10].

Reinforcing particles are relatively easy to infiltrate during compocasting process and so the problem of wettability [11] is not necessary to solve. It is possible to infiltrate various reinforcing particles (SiC, Al_2O_3, TiB_2 etc.) in the metal matrix (aluminium alloys [3], magnesium alloys [12], zinc–aluminium alloys etc.). The particles of ash [13], graphite [14] or some other solid lubricant have been also used in order to improve tribological characteristics of base alloys. With suitable combination of process parameters it is possible to achieve a very good distribution of reinforcing particles in the composite matrix and thus affect mechanical properties of the composite. During compocasting process composite materials can be produced in the form of so-called thixo ingots, which can be

* Corresponding author. Tel.: +381 11 33 02 291; fax: +381 11 33 70 364.
E-mail addresses: avencl@mas.bg.ac.rs (A. Vencl), ilijab@vinca.rs (I. Bobic), saioa.arostegui@csm-instruments.com (S. Arostegui), biljanabobic@gmail.com (B. Bobic), amarinkovic@mas.bg.ac.rs (A. Marinković), babic@kg.ac.rs (M. Babić).

0925-8388/$ – see front matter © 2010 Elsevier B.V. All rights reserved.
doi:10.1016/j.jallcom.2010.07.028

Table 1
Chemical composition (wt.%) of A356 aluminium alloy.

Element	Si	Cu	Mg	Mn	Fe	Zn	Ni	Ti	Al
Percentage	7.20	0.02	0.29	0.01	0.18	0.01	0.02	0.11	Balance

subsequently processed using a variety of techniques, e.g. vortex processing, squeeze casting [4] or extrusion [15].

The aim of this work was to make particulate composites with A356 aluminium alloy as the composite matrix applying compocasting process and using different reinforcing particles (Al_2O_3, SiC) and graphite particles. Comparison of structural, mechanical and tribological properties of the obtained composites with the matrix alloy and between themselves was also the aim of this work.

2. Experimental procedure

2.1. Producing of composites

Hypoeutectic A356 aluminium alloy (hereafter referred as A356) was used as the basis for obtaining composites. Chemical composition of the alloy is given in Table 1.

The composites were produced by compocasting process. The amount of infiltrated particles was 10 wt.% for Al_2O_3 and SiC particles and 1 wt.% for graphite particles, while the size of particles was approximately equal. The obtained composite materials were as follows:

- A356 aluminium alloy + 10 wt.% Al_2O_3 (35 μm particles size),
- A356 aluminium alloy + 10 wt.% SiC (39 μm particles size) and
- A356 aluminium alloy + 10 wt.% SiC (39 μm particles size) + 1 wt.% graphite (35 μm particle size).

The composites were designed in further text as the composites C1, C2 and C3, respectively.

Parameters of compocasting were the same for all composites as well as the parameters of hot pressing and heat treatment so the comparison of structural, mechanical and tribological properties of the obtained composite materials was possible.

Infiltration of reinforcing particles and graphite particles into the semi-solid melt of the matrix alloy was performed using the laboratory equipment described previously [16]. Ceramic reinforcing particles (Al_2O_3 and SiC) were preheated at 150 °C to eliminate moisture and reduce thermal stress at the beginning of infiltration. In the case of dual composite C3 (with SiC and graphite particles) SiC and graphite were mixed (before infiltration) in the solid state, and then preheated at 150 °C. A356 aluminium alloy was entered in the previously preheated crucible of electro-resistance furnace, melted and overheated to 650 °C (area of liquid phase) to clean the slag. The alloy melt was then cooled down to 600 °C to obtain the semi-solid melt and this temperature was kept constant during 10 min before the infiltration of particles started. Isothermal mixing of the alloy semi-solid melt (at 600 °C) was performed using paddle stirrer at rotation frequency of 500 rpm. The mixing lasted for 5 min to break dendritic structure that was formed during cooling of the melt from 650 to 600 °C and to facilitate the infiltration of particles.

Infiltration was carried out continuously during 7 min. The particles were added into the melt zone next to the shaft of stirrer at rotation frequency of 500 rpm. During infiltration the temperature of the melt was gradually risen up to 610 °C in order to facilitate infiltration, because of viscosity increase with the addition of particles. Mixing of the composite semi-solid melt after infiltration of particles was done in two phases. In the first one mixing was performed at rotation frequency of 1000 rpm for 2 min. During this phase the process was stabilized and temperature of the semi-solid melt achieved 600 °C. During second phase that lasted for 5 min mixing was carried out at rotation frequency of 1500 rpm in isothermal mode, at the temperature of 600 ± 3 °C. Semi-solid melts of composites were poured into the steel mould preheated at 500 °C. Obtained composite castings were prismatic (20 mm × 30 mm × 100 mm). These castings were machined and prismatic samples (7 mm × 7 mm × 30 mm) were obtained. The samples were hot pressed at 570 °C with 60 kN force using a special tool [16]. In this way cylindrical samples were obtained with 6 mm in diameter and 20 mm in height. These samples were machined to 5 mm in diameter and 20 mm in height to obtain specimens for structural examination and hardness test and specimens for fractographic and tribological studies.

Specimens of the composites and of matrix A356 aluminium alloy were thermally processed applying T6 heat treatment regime, which consists of solution annealing at 540 °C for 6 h, water quenching and artificial aging at 160 °C for 6 h.

2.2. Methods of characterization

Metallographic examinations were carried out using Zeis Axiovert optical microscope (OM). Specimens were wet ground using abrasive SiC paper (240, 360, 600 and 800 grit, respectively). Polishing was performed on a polishing cloth using diamond paste (2 μm particles size). Etching of specimens was carried out using the Keller's solution (2.5 mL HNO_3 + 1.5 mL HCl + 1 mL HF + 95 mL H_2O).

Fractographic examinations were performed applying Jeol JSM-5800 scanning electronic microscope (SEM).

Determining of elasticity modulus was done using CSM micro-indentation tester and applying the Instrumented indentation technique [17,18] under the assumption that all tested materials have Poisson's ratio of 0.3. The scheme of the CSM device is given in Fig. 1.

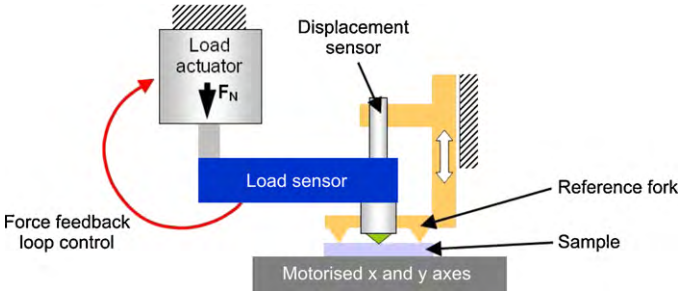

Fig. 1. The scheme of the micro-indentation tester.

The micro-indentation tester uses an already established method where an indenter tip with a known geometry is driven into the specific site of the material to be tested, by applying an increasing normal load. When reaching the pre-set maximum value, the normal load is reduced until partial or complete relaxation occurs. At each stage of the experiment the position of the indenter relative to the sample surface is precisely monitored with a differential capacitive sensor. This procedure was performed repetitively in ambient air, at temperature of 23 °C and humidity of 40%. The following indentation parameters were used to produce several indents on each sample (six to twelve depending on the tested material): indenter Vickers; contact load 10 mN; loading rate 2 N/min; maximum load 1 N and pause at maximum load 15 s.

Microhardness was measured using Buehler IndentaMet 1100 Series semi-macro- and macro-Vickers indentation hardness tester with 300 g load. At least

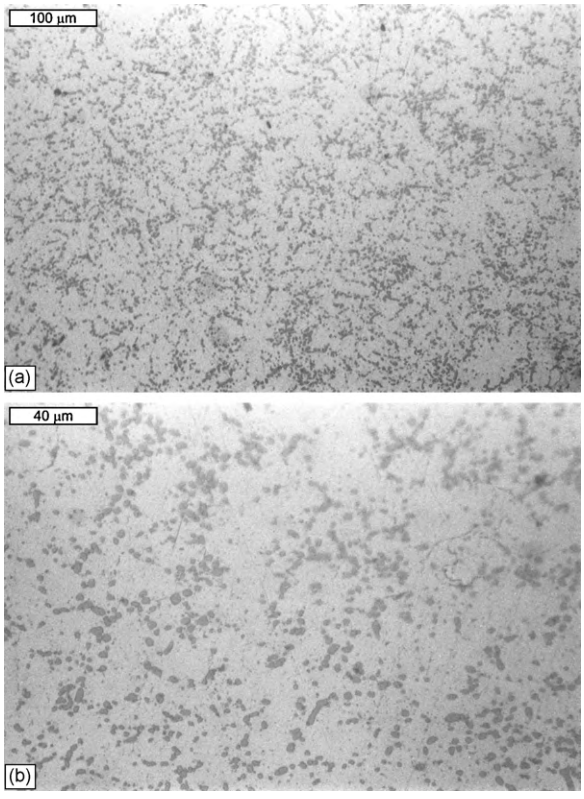

Fig. 2. The structure (OM) of heat treated (T6) A356 aluminium alloy.

six measurements were made for each specimen in order to eliminate possible segregation effects and to get a representative value of the material microhardness.

Tensile tests were performed using Instron M 1185 tensile machine. The values of yield strength ($R_{p0.2}$) were determined applying the engineering stress–strain curve (this is constructed from load-elongation measurements) [19].

Tribological tests were carried out on the CSM pin-on-disc tribometer under dry sliding conditions, in ambient air, at temperature of 23 °C and humidity of 40%. Tribometer test mode was linear (reciprocating) movement. Moving body (test sample) was made from tested materials while the static body (counter body) was an alumina ball. Total wear track length on the reciprocating moving test samples was 5 mm. Maximum test samples velocity was 0.06 m/s and the average one was ~0.038 m/s. Stop condition for all tests was 50,000 cycles i.e., after 1.31×10^4 s, which gave a total sliding distance of 500 m. The constant normal load of 1 N was maintained during all tests.

Before testing, both the test sample and the counter body were degreased and cleaned with isopropyl alcohol. The wear volume of the test samples was measured at the end of testing with Taylor Hobson profilometer. The value of friction force was monitored during the test and through data acquisition system stored in the PC, enabling the calculation of friction coefficient. Worn surfaces of counter body and test samples were observed after testing using OM and SEM.

3. Results and discussion

3.1. Microstructural examination

The structure of T6 heat treated A356 aluminium alloy is presented in Fig. 2. Significant morphological changes can be noticed in relation to the as cast structure, which was obtained by casting in a graphite mould [16]. Dendritic structure was transformed during the heat treatment process and the silicon sticks (a part of eutectic) were transformed into circular or elliptical nodules. These nodules have created the boundaries of α phase. A fine microstructure of heat treated A356 aluminium alloy was achieved.

Microstructures of the obtained composites are shown in Fig. 3. Microstructure of composite C1 (with Al_2O_3 particles) is shown in Figs. 3a and b. Reinforcing particles are arranged in clusters of type A [20]. Fine nodules of silicon can be seen next to these particles. During compocasting process the structure coarsening took place i.e., the expansion of α phase area occurred.

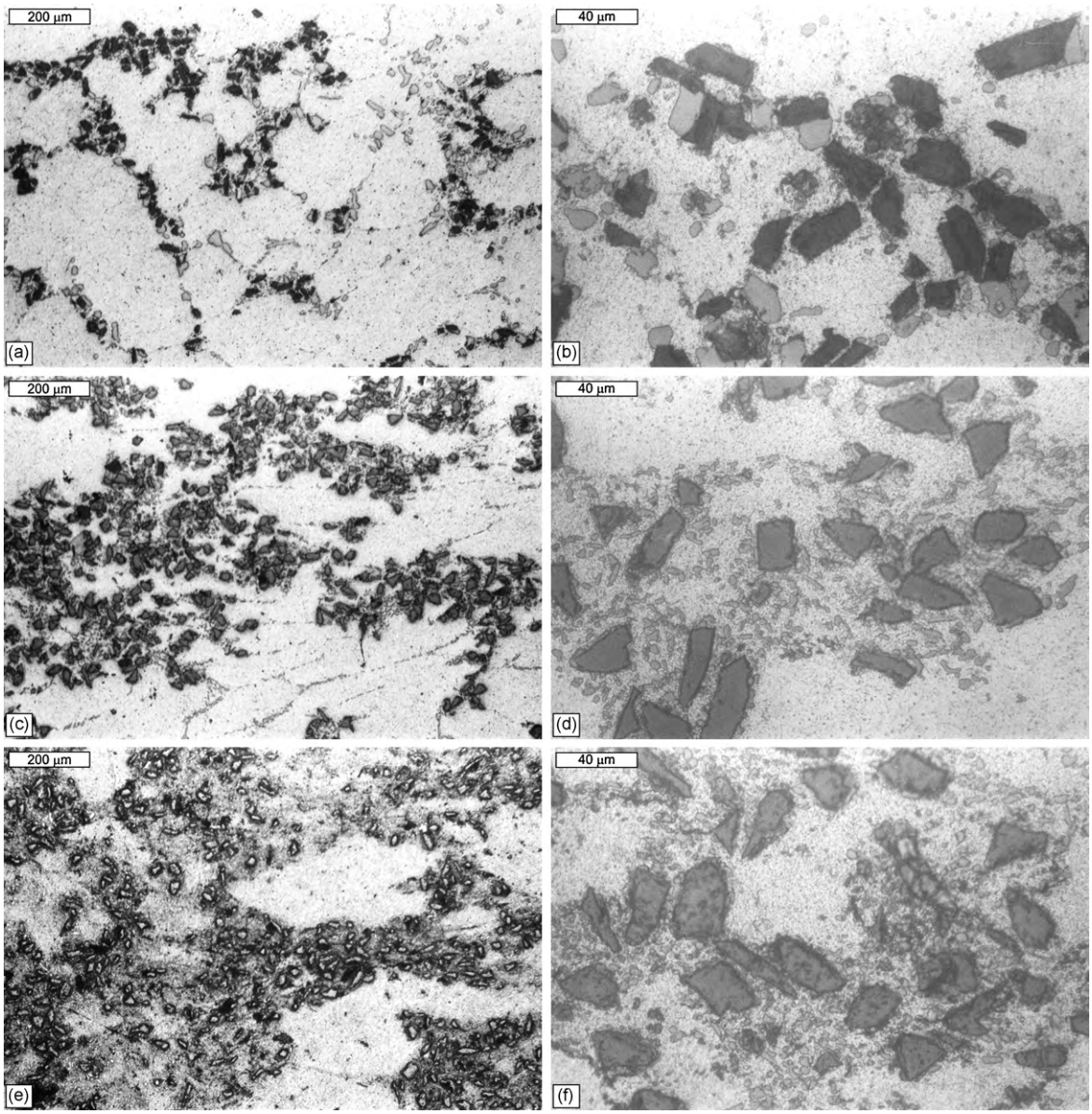

Fig. 3. The structures (OM) of heat treated (T6) composite (a) and (b) C1 (with 10 wt.% Al_2O_3), (c) and (d) C2 (with 10 wt.% SiC) and (e) and (f) C3 (with 10 wt.% SiC and 1 wt.% graphite).

From Fig. 3a might be concluded that Al_2O_3 particles were dispersed in the liquid phase during mixing of semi-solid melt. After the mixing was stopped and temperature of the melt was decreased the reinforcing particles were trapped on the boundaries of large primary particles of α phase. During heat treatment of the composite C1 the silicon sticks were transformed into silicon nodules. Silicon particles are mainly located in the vicinity of Al_2O_3 particles (Fig. 3a). Position of reinforcing Al_2O particles in the clusters can be seen more clearly in Fig. 3b. The debonding effect was not observed at this level of examination although there is a contact between silicon particles and Al_2O_3 particles here and there. Fig. 3b also shows that there is a good mechanical bond between Al_2O_3 particles and the matrix alloy. This can be stated because of absence of dimples that usually appear in the case of poor mechanical bond between reinforcing particles and composite matrix.

Microstructure of the composite C2 (with SiC particles) is shown in Fig. 3c and d. Clusters of reinforcing particles are of type B [20]. It is noticeable that the area with reinforcing particles was extended, while the area without particles became smaller, indicating better distribution of SiC particles (Fig. 3c) in the composite matrix in comparison to the distribution of Al_2O_3 particles (Fig. 3a). During mixing SiC particles were placed not only in the liquid phase but also in the solid phase of the semi-solid melt. After the mixing was stopped, these particles were entrapped in both liquid and solid phase. It can be noticed that silicon nodules are placed in the vicinity of SiC particles (Fig. 3d). The more uniform distribution of SiC particles and the debonding effect (Fig. 3d) are complex phenomena and they need further analysis which was not done at this level of examination.

Microstructure of the composite C3 (with SiC and graphite particles) is shown in Figs. 3e and f. This structure (Fig. 3e) is very similar to the structure of composite C2 (Fig. 3c). Soft graphite particles did not keep their average size (35 μm) during compocasting. Their fracturing and smearing occurred already during preparation (mixing with SiC particles in solid phase) and were continued during mixing in the process of compocasting (collisions with SiC particles, with the active part of stirrer and with crucible walls). Graphite particles of different size and graphite layers are visible in Fig. 3e and f.

3.2. Fractographic examination

Fracture appearance of heat treated (T6) sample of A356 aluminium alloy is shown in Fig. 4. The fracture can be characterized as ductile with clearly marked serpentine glides. The presence of dimples is not observed at higher magnification (Fig. 4b). Silicon

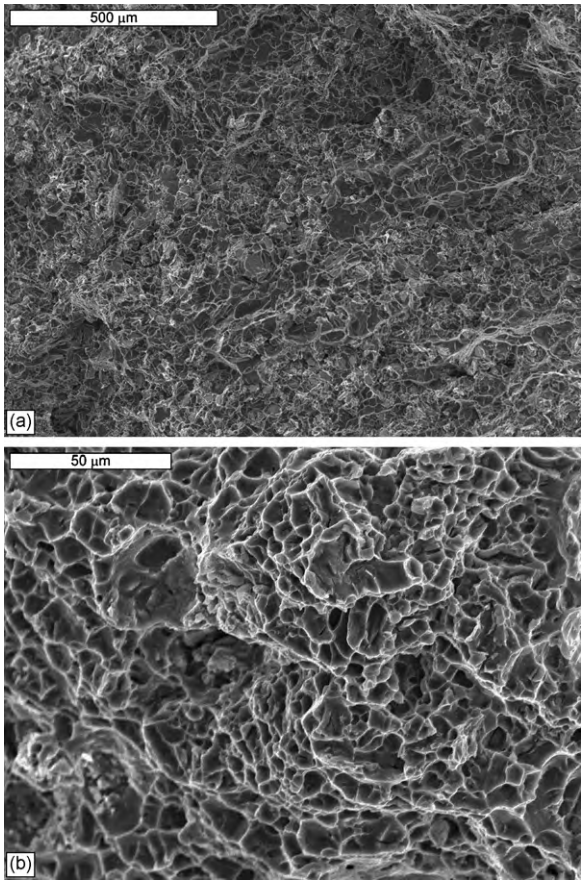

Fig. 4. SEM fractographs of heat treated (T6) A356 aluminium alloy.

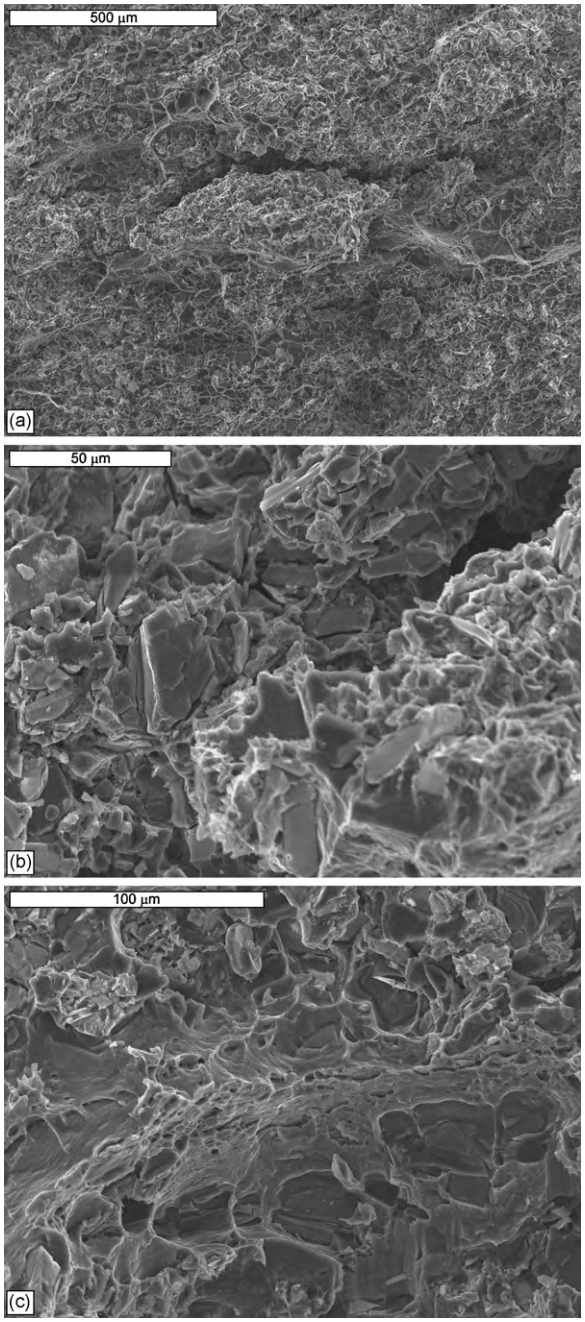

Fig. 5. SEM fractographs of heat treated (T6) composite C1 (with 10 wt.% Al_2O_3).

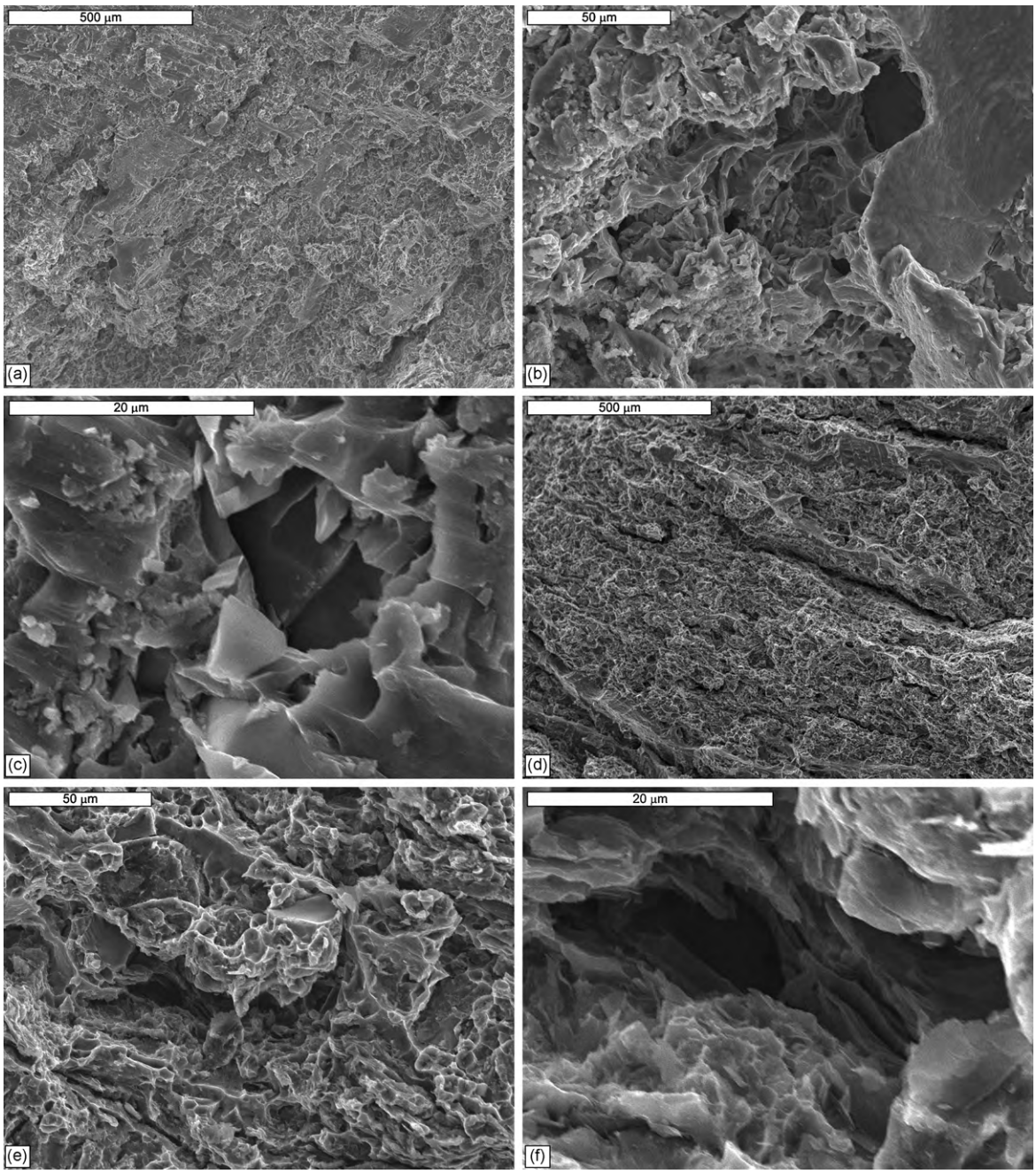

Fig. 6. SEM fractographs of heat treated (T6) composites (a)–(c) C2 (with 10 wt.% SiC) and (d)–(f) C3 (with 10 wt.% SiC and 1 wt.% graphite).

particles are firmly attached to α phase (aluminium). The process of plastic deformation occurred by sliding of α phase planes.

The fracture appearance of composites was different compared to the fracture appearance of A356 aluminium alloy. The fracture appearance of the composite C1 (with Al_2O_3 particles) is presented in Fig. 5.

The composite matrix shows characteristics of ductile fracture. However, the appearance of cracks can be observed in the zone of clusters (Fig. 5b). These cracks propagate along the interface between reinforcing particles and matrix which means that debonding and fracture takes place along the interface. The intergranular fracture in the zone of clusters is brittle. The appearance of fracture surface indicates good mechanical bond between reinforcing particles and matrix because the dimples were not observed (Fig. 5b). The existence of dimples would be indicated by fall out of reinforcing particles from the matrix during the fracture of a sample. Besides, the microcracks on reinforcing particles are visible (Fig. 5b). This is caused by thermal shock during water quenching of composites due to different coefficients of thermal expansion for reinforcing particles and matrix. Ductile fracture of the composites matrix was confirmed by the fracture appearance in Fig. 5c. The flow lines of aluminium can be seen.

Morphologies of the fracture surfaces of composite C2 (with SiC particles) and composite C3 (with SiC and graphite particles are similar (Fig. 6a and d). Transition from ductile to intergranular fracture occurs in the zone of reinforcing particles where appearance of microcracks was observed. However, at higher magnification (Figs. 6b and e) dimples can be seen in the case of composite C2. Shape and dimension of the dimples match the shape and dimension of reinforcing particles (Fig. 6c). This points out to worse mechanical bond between SiC particles and matrix in comparison to the bond between Al_2O_3 particles

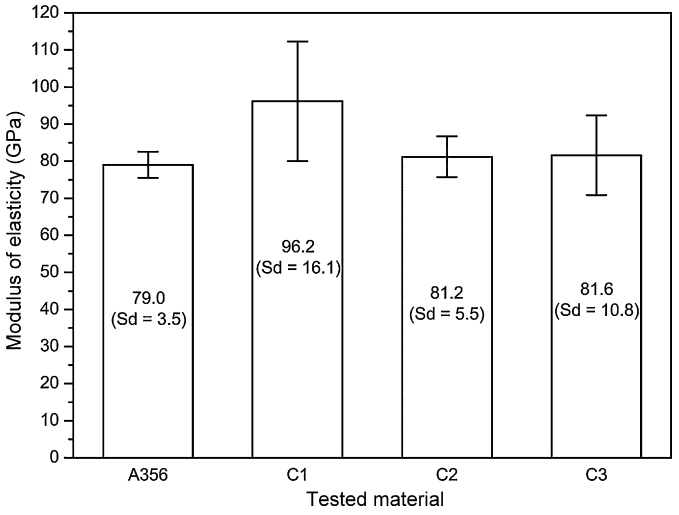

Fig. 7. Modulus of elasticity value of heat treated (T6) A356 aluminium alloy, composite C1 (with 10 wt.% Al_2O_3 particles), composite C2 (with 10 wt.% SiC particles) and composite C3 (with 10 wt.% SiC and 1 wt.% graphite particles).

and matrix. A similar phenomenon can be seen in the case of composite C3 (Fig. 6f). It was not possible to determine the influence of graphite itself to the composite fracture at this level of examination.

3.3. Mechanical properties

In metal matrix composites, mechanical properties depend on the mechanical properties of the matrix material and the nature of the interface as well as on the amount, size, shape and distribution of the dispersed phase [10].

Values of elasticity modulus of heat treated matrix alloy and composites are shown in Fig. 7.

It can be seen that all composites have higher values of elasticity modulus in relation to the A356 aluminium alloy. The value of elasticity modulus is the highest in the case of composite C1 (with Al_2O_3 particles), while it is lower for the composites C2 (with SiC particles) and C3 (with SiC and graphite particles). A356 aluminium alloy has the lowest value of elasticity modulus. These results point to the fact that the substantial change of material properties has occurred in the composites, and that change depends only on the bond strength between atoms [19]. Comparing the values of elasticity modulus for composites C1 and C2 it can be concluded that the arrangement of reinforcing particles does not significantly affect them which is consistent with the results reported by Tszeng [20]. In composite C1 Al_2O_3 particles are distributed in the clusters of type A (Fig. 3a) with segregated particles-rich regions (clusters) and particles free regions. On the other hand in composite C2 and C3 SiC particles are distributed in the clusters of type B (uniformly dispersed particles with few isolated clusters) which is favourable for plastic properties of the composite. The results of fractographic examinations within this work have also indicated higher bond strength between reinforcing particles and matrix in the case of composite C1.

Beside the modulus of elasticity, hardness and yield strength of the matrix alloy and obtained composites were determined and shown in Table 2. It can be seen that the arrangement of reinforcing particles and graphite addition have much bigger influence on the plastic behaviour in relation to the elastic behaviour of the examined materials. Hardness value increases with addition of Al_2O_3 particles, while the yield point slightly decreases in relation to the matrix alloy. With addition of SiC particles a significant increase in hardness and yield strength value can be observed. Values of these mechanical characteristics decrease with addition of SiC and graphite particles together.

Table 2
Mechanical properties of heat treated (T6) A356 aluminium alloy and composites.

Material	Microhardness ($HV_{0.3}$)	Yield strength $R_{p0.2}$ (MPa)
A356 aluminium alloy	65.8	190
Composite C1 (with 10 wt.% Al_2O_3)	76.7	187
Composite C2 (with 10 wt.% SiC)	82.8	198
Composite C3 (with 10 wt.% SiC and 1 wt.% graphite)	62.1	170

3.4. Tribological properties

Tribological investigation of these materials was just an initial one, with preliminary results and some more experiments to be done to completely understand their tribological behaviour. In order to achieve a higher confidence level in evaluating test results, three to four replicate tests were run for all the tested materials.

Obtained average values of the wear testing are presented in Fig. 8. The highest value showed A356 aluminium alloy, then composite C1 (with Al_2O_3 particles), composite C2 (with SiC particles), and the lowest wear showed composite C3 (with SiC and graphite particles). These results are in correlation with the hardness values of the tested materials (Table 2), except for the composite C3. The A356 aluminium alloy showed lower wear than it could be expected since it was not reinforced. Wear resistance of as cast A356 aluminium alloy is affected by silicon particles in the form of sticks [16] that were created as a result of eutectic reaction during the alloy solidification. Higher wear resistance of heat treated samples of A356 aluminium alloy in comparison to as cast samples is the result of significant structural changes during T6 heat treatment. During aging phase of T6 regime the hardening of the alloy structure (age hardening) takes place due to creation of fine deposits of β' phase (Mg_2Si) [21]. In addition, silicon sticks are transformed into silicon nodules that prevent shearing of α phase layers. Also, during heat treatment process the inhomogeneous dendritic structure of the matrix was decomposed and the creation of a fine structure has occurred (Fig. 2). The uniformity of mechanical and tribological properties is the consequence of this structure.

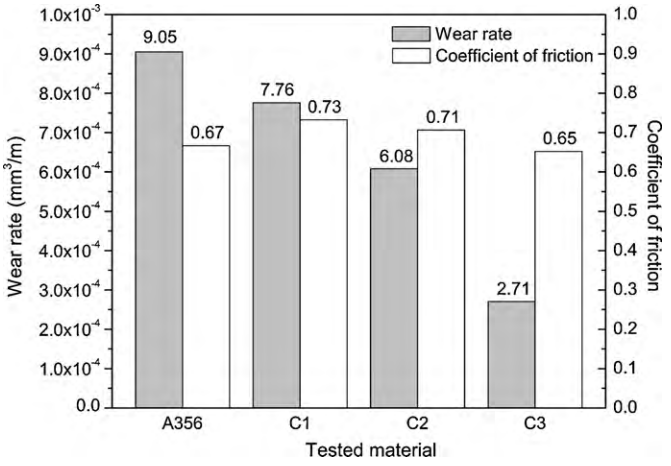

Fig. 8. Wear rate and coefficient of friction values of heat treated (T6) A356 aluminium alloy, composite C1 (with 10 wt.% Al_2O_3 particles), composite C2 (with 10 wt.% SiC particles) and composite C3 (with 10 wt.% SiC and 1 wt.% graphite particles); coefficient of friction values are for the steady state period—after 300 m.

Table 3
Obtained average values of the running-in distance from the friction testing.

Material	Running-in distance (m)
A356 aluminium alloy	200
Composite C1 (with 10 wt.% Al_2O_3)	270
Composite C2 (with 10 wt.% SiC)	170
Composite C3 (with 10 wt.% SiC and 1 wt.% graphite)	130

In the case of composite C1 structure of the composite matrix was non-dendritic but coarser than the structure of A356 aluminium alloy, as a result of compocasting process. The zones of α phase occupy larger areas in the composite matrix. The effects of strengthening due to a difference in thermal expansion coefficients of the matrix and reinforcing particles [22] are the most expressive around the clusters so that the surface residual stresses are not uniform. This influenced the dissipation of results in microhardness test, which amounted up to $\pm 10\ HV_{0.3}$ in our experiments compared to the average values (Table 2) as well as the dispersion of tribological results. The composite C1 had higher wear resistance compared to A356 aluminium alloy (Fig. 8) due to the presence of the hard reinforcing particles.

Higher wear resistance of the composites reinforced with SiC particles in relation to the composite reinforced with Al_2O_3 particles is in correlation with research conducted by Rohatgi et al. [10]. This can be explained by the favourable arrangement of SiC reinforcing particles in the composite matrix, i.e. the area without particles in the matrix is reduced, which have caused more uniform wear and better protection of the surface. Also the hardness of the SiC particles is higher. Basavarajappa et al. [23] investigated dry sliding wear behaviour of base aluminium alloy 2219 and composite with SiC and graphite particles, fabricated using the liquid metallurgy technique. SiC and graphite particles had an average size of 25 and 45 μm, respectively. They found that the addition of SiC and graphite particles increases the wear resistance of the composites comparing to the matrix alloy. They also found that addition of even relatively small amount of graphite (3%) to the composite with SiC particles increases the wear resistance of the composites. During the sliding protruded SiC particles fracture and lead to the abrasive wear. However, at places where graphite particles are present, the fractured SiC particles easily penetrate into the matrix alloy due to the low hardness, squeezing some of the graphite from the matrix. The graphite particles smear at the interface between the contact bodies and reduce the coefficient of friction. Hence, the heat generated due to friction is also reduced. On the other hand the graphite also lowers the hardness of the material, which explains the relatively low hardness values of the composite C3 (Table 2). Mohan et al. [24] found that in a dry sliding test of composite with aluminium matrix and addition of graphite particles, graphite smears at the sliding interface and reduces wear, but graphite addition beyond 1.5% reduces the mechanical properties of the composite.

Results of the friction testing are presented in Fig. 8 and Table 3. From Table 3 it can be noticed that the running-in period was not the same for all tested materials. The longest running-in period was noticed for composite C1, and the shortest for the composite C3. The shortest value, noticed at composite C3, is expected since this composite contained graphite which acts as a solid lubricant, but the value for A356 aluminium alloy was lower than expected. The reason for this could be a plastic flow of the material and its transfer to the counter body (Fig. 11).

Attained values of the coefficient of friction were in expected range for light metals in dry sliding conditions, and all tested materials showed very similar values of friction coefficient (Fig. 8). The biggest value showed composite C1. Higher values of the coefficient of friction for composites compared to the A356 aluminium alloy are ascribed to the fact that the amount of protruded reinforcement particles increases during wear occupying larger area of tested sample surface. At the same time a part of protruded particles is torn away from the matrix and fractured into fragmented pieces. In this situation the contact between hard reinforcement particles and the counter body material was established, resulting in higher values of the coefficient of friction. A relatively lower friction coefficient value of the A356 aluminium alloy is also due to the fact that at applied specific load sample surfaces of this material start to deform plastically and to flow (Fig. 9a).

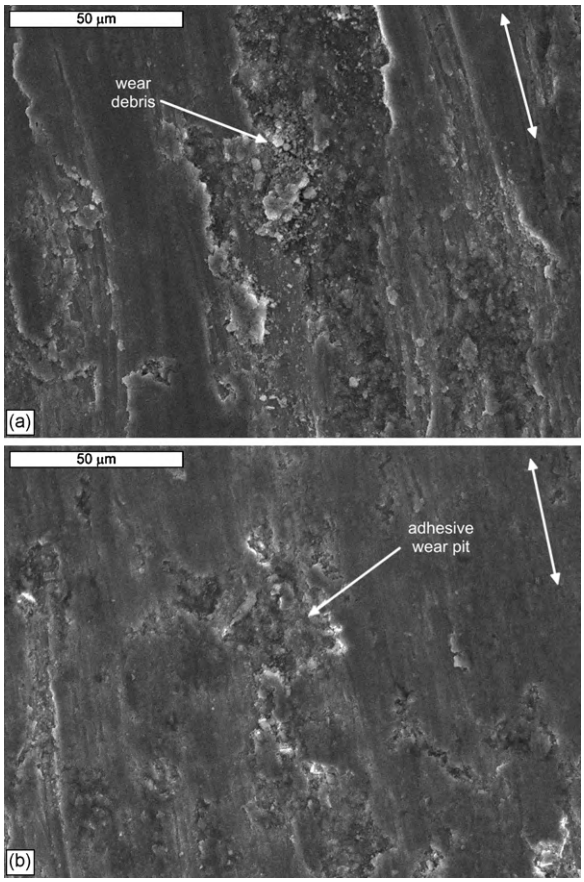

Fig. 9. SEM micrographs of test samples worn surfaces (a) A356 aluminium alloy and (b) composite C1 (with 10 wt.% Al_2O_3 particles); sliding directions is denoted with double arrows.

Values of the coefficient of friction for composites correspond to the wear rate values of those materials (Fig. 8). Generally for all composites values of friction coefficient were higher compared to the A356 aluminium alloy. An exception is the composite C3 probably due to the fact that small amount of graphite (1 wt.%) was present in this composite. Since the presence of graphite was small this should be considered with caution and only noticed as a possible trend of behaviour. A supplement to this could be a research of Yang et al. [14] where they found that for composites with graphite in small content (around 2 wt.%) the formed lubricant film could not effectively decrease the coefficient of friction. They also found that increasing of the graphite addition up to some value (6 wt.%) decrease the coefficient of friction and wear rate, but greater amount of graphite does not show further significant improvements of the coefficient of friction and even tends to increase the wear rate of composite. In their case the average graphite particle size was 15 μm and in our study original graphite particles average size was 35 μm and did not keep their average size during compocasting (see Section 3.1).

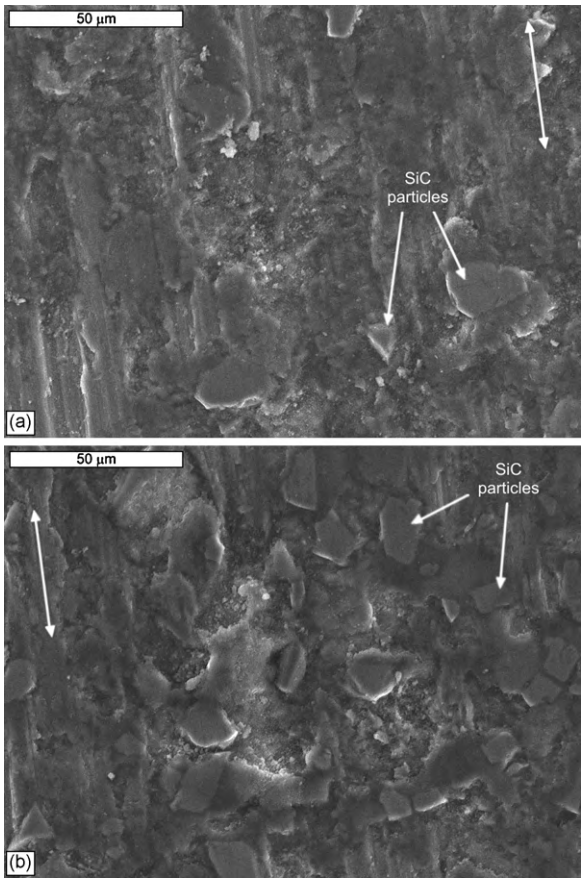

Fig. 10. SEM micrographs of test samples worn surfaces (a) composite C2 (with 10 wt.% SiC particles) and (b) composite C3 (with 10 wt.% SiC and 1 wt.% graphite particles); sliding directions is denoted with double arrows.

It is commonly known that the size of the particles for composites that contain soft particles affects the wear rates and coefficients of friction of composites under sliding wear conditions i.e., the larger the particles, the lower the wear rate and coefficient of friction [10]. It is also well known that the effect of sliding velocity on wear rate is more complex for composites that contain soft particles. Rohatgi et al. [10] in their article specify an example that the wear rate for an aluminium alloy composite containing 5% graphite decreases with increasing sliding speed (0.5–5 m/s), which is applicable to this study since the sliding speed in our case was relatively small (~0.038 m/s). It is obvious that for each case and application exists a range of optimal value of graphite particle content which gives material with good tribological properties.

Characterization of the microstructure of wear surface for metal matrix composites is more complex than that of the metals or alloys and an understanding of wear mechanisms is far from complete. The SEM analysis of wear surface was carried out to disseminate the wear mechanisms of the tested materials. SEM micrographs presented in Figs. 9 and 10 are taken at the end of tests. Worn surfaces of A356 aluminium alloy (Fig. 9a) and composite C1 (Fig. 9b) showed similar appearance. Significant smearing as a result of material plastic flow could be noticed on both material but this smearing was less pronounced for composite C1. This corresponds to the wear rate values of these two materials. Dominant type of wear was adhesive wear with adhesive plates of deformed material and presence of wear debris caused by fracture, accumulated into the adhesive wear pits (denoted by arrows in Fig. 9). Presence of the reinforcement (Al_2O_3) particles on the surface of composite C1 was not noticed. For the composites C2 and C3 dominant type of wear was also adhesive wear. Distinction of those two composites worn

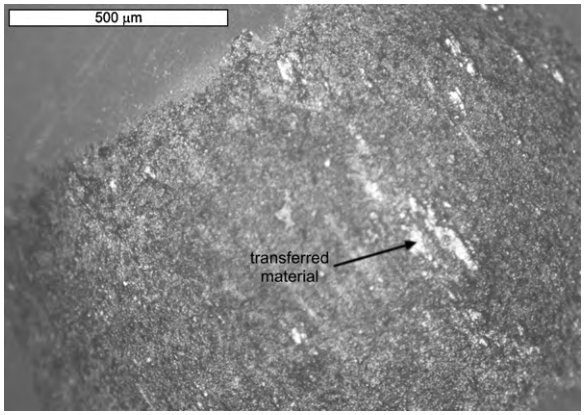

Fig. 11. OM micrograph of the counter body worn surface (a counter body in contact with A356 aluminium alloy).

surfaces appearance from the composite C1 is presence of the protruded reinforcement particles (SiC particles in this case). Presence of those particles was more obvious for the composite C3 than for the composite C2 (Fig. 10). The fact that the reinforcements were protruded to the surface and thus protect the matrix alloy from further wear reflect on the wear rates of those two composites which were smaller than wear rates of the A356 aluminium alloy and composite C1. On the surface of the counter body which was observed with OM presence of transferred material was noticed, and this transfer was more obvious for the contact with A356 aluminium alloy (Fig. 11).

4. Conclusions

The composite materials with better mechanical and tribological properties in relation to matrix A356 aluminium alloy can be obtained by compocasting process.

Reinforcing particles (Al_2O_3, SiC) were arranged in clusters in the composite matrix. The arrangement of SiC particles in clusters was more favourable for mechanical and tribological properties of the composite in comparison to the arrangement of Al_2O_3 particles. The debonding effect was not observed between reinforcing particles and the matrix alloy at this level of examination. Soft graphite particles did not keep their average size during compocasting process.

The fracture of the composite matrix (A356 aluminium alloy) can be characterized as ductile. In the case of composites, a transition from the ductile to a brittle, intergranular fracture occurred in the zone of reinforcing particles.

Wear resistance of the composites reinforced with SiC particles was higher and coefficient of friction was lower than the wear resistance and coefficient of friction of the composite reinforced with Al_2O_3 particles due to the favourable arrangement of SiC reinforcing particles in the composite matrix, and due to the higher hardness of the SiC particles. Addition of graphite particles (1 wt.%) to the composite with SiC particles further reduced the wear rate and the coefficient of friction, but this influence, of such relatively small amount of graphite, was not clear enough and should be considered only as a trend of behaviour.

It seems useful to continue the work on developing dual composites with A356 aluminium alloy as the matrix in order to obtain composite materials with favourable combination of structural, mechanical and tribological properties.

Acknowledgements

This work has been performed within the project TR-14005. This project is supported by the Republic of Serbia, Ministry of Science

and Technological Development, which financial help is gratefully acknowledged.

References

[1] A. Kearney, E.L. Rooy, ASM Handbook, vol. 2, ASM International, Metals Park, 1990, pp. 123–151.
[2] R. Pešić, S. Veinović, R. Pavlović, Mobility & Vehicles Mechanics 30 (2004) 65–84.
[3] P. Rohatgi, JOM 42 (1991) 10–15.
[4] H. Ribes, M. Suéry, Scripta Metallurgica 23 (1989) 705–709.
[5] A. Daoud, W. Reif, Journal of Materials Processing Technology 123 (2002) 313–318.
[6] R. Mehrabian, R.G. Riek, M.C. Flemings, Metallurgical and Materials Transactions B 5 (1974) 1899–1905.
[7] A.M. Hassan, A. Alrashdan, M.T. Hayajneh, A.T. Mayyas, Tribology International 42 (2009) 1230–1238.
[8] S. Naher, D. Brabazon, L. Looney, Journal of Materials Processing Technology 143–144 (2003) 567–571.
[9] M. Rosso, Journal of Materials Processing Technology 175 (2006) 364–375.
[10] P.K. Rohatgi, Y. Liu, S. Ray, in: P.J Blau (Ed.), ASM Handbook, vol. 18, ASM International, Metals Park, 1992, pp. 801–811.
[11] S. Naher, D. Brabazon, L. Looney, Journal of Materials Processing Technology 166 (2005) 430–439.
[12] G. Sasaki, M. Yoshida, N. Fuyama, T. Fujii, Journal of Materials Processing Technology 130–131 (2002) 151–155.
[13] T.P.D. Rajan, R.M. Pillai, B.C. Pai, K.G. Satyanarayana, P.K. Rohatgi, Composites Science and Technology 67 (2007) 3369–3377.
[14] J.B. Yang, C.B. Lin, T.C. Wang, H.Y. Chu, Wear 257 (2004) 941–952.
[15] R. Rahmani Fard, F. Akhlaghi, Journal of Materials Processing Technology 187–188 (2007) 433–436.
[16] A. Vencl, I. Bobić, M.T. Jovanović, M. Babić, S. Mitrović, Tribology Letters 32 (2008) 159–170.
[17] N. Randall (Ed.), Applications Bulletin, no. 18, CSM Instruments, Peseux, 2002, pp. 1–4 http://www.csm-instruments.com/en/tests-Standards.
[18] A.R. Franco Jr, G. Pintaúde, A. Sinatora, C.E. Pinedo, A.P. Tschiptschin, Materials Research 7 (2004) 483–491.
[19] G.E. Dieter, Mechanical Metallurgy, McGraw-Hill, New York, 1963.
[20] T.C. Tszeng, Composites Part B: Engineering 29 (1998) 299–308.
[21] R.X. Li, R.D. Li, Y.H. Zhao, L.Z. He, C.X. Li, H.R. Guan, Z.Q. Hu, Materials Letters 58 (2004) 2096–2101.
[22] R.J. Arsenault, L. Wang, C.R. Feng, Acta Metallurgica et Materialia 39 (1991) 47–57.
[23] S. Basavarajappa, G. Chandramohan, K. Mukund, M. Ashwin, M. Prabu, Journal of Materials Engineering and Performance 15 (2006) 668–674.
[24] S. Mohan, J.P. Pathak, R.C. Gupta, S. Srivastava, Zeitschrift für Metallkunde 93 (2002) 1245–1251.